ChemComm

Check for updates

Dual supramolecular chirogenesis based on platinum(II) metallotweezers†

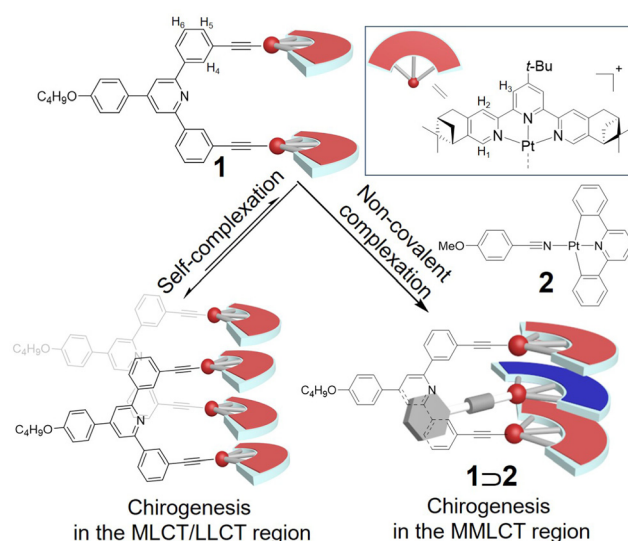Jie Ren, [a] Sixun Jiang, [b] Tingting Han, [a] Shuai Wu, [a] Yukui Tian*[ac] and Feng Wang *[b]

Optically active platinum(II) metallotweezers demonstrate both self-complexation and host–guest complexation capabilities, leading to two distinct supramolecular chirogenic signals in the visible region.

Chirality transfer from the molecular level to the supramolecular level is not only essential in life[1] but is relevant for catalytic, optoelectronic and spintronic applications in materials science.[2] Supramolecular chirogenesis[3] represents an efficient way to express chirality in artificial systems, and involves non-covalent chiral recognition between the host and guest species. Pioneering work in this field has been performed by Inoue and co-workers on the basis of achiral zinc porphyrin tweezers.[3a,c] Until now, supramolecular chirogenesis has extended to various artificial receptors such as macrocycles,[4] cages,[5] and helical foldamers.[6] Despite the progress achieved, the chirogenic signals appear primarily in the ultra-violet or high-energy visible region due to the following two reasons. One is the lack of large π-conjugated chromophores on host/guest structures, and the other is the low chirality transfer efficiency because of the remoteness of the chiral center from the host–guest complexation site.[7] It is intriguing to shift supramolecular chirogenic signals to a low-energy absorption region, which would benefit circular polarized light detection/emission and chiroptical switch applications.

Platinum(II)-based metallotweezers,[8] with two cofacial square-planar pincers, represent an ideal candidate to attain this objective. When the cyclometalated Pt(II) pincers are kept

at the distance of 7 Å by a rigid spacer, the metallotweezers are capable of encapsulating a guest molecule into their cavity.[9] The non-covalent host–guest complexation structure is stabilized by π–π stacking interactions between the Pt(II) pincers and the complementary guest (interplanar distance: ∼3.5 Å). It can be endowed with fruitful photo-physical properties due to the spin–orbit coupling effect, leading to metal-to-ligand charge transfer (MLCT), ligand-to-ligand charge transfer (LLCT), and metal–metal-to-ligand charge transfer (MMLCT) transitions in the low-energy absorption region.[10] We envisage that supramolecular chirogenic signals could potentially emerge for these electronic transitions, by incorporating a stereogenic center in the receptor of the metallotweezers.

In this study, we have designed the novel Pt(II) metallotweezers **1** (Scheme 1, see Scheme S1 in the ESI† for the synthetic procedure). Unlike previous chiral Pt(II) complexes in which the

[a] *Institutes of Physical Science and Information Technology, Anhui University, Hefei, Anhui, 230601, China. E-mail: tianyk@ahu.edu.cn*

[b] *Key Laboratory of Soft Matter Chemistry, Department of Polymer Science and Engineering, University of Science and Technology of China, Hefei, Anhui, 230026, China. E-mail: drfwang@ustc.edu.cn*

[c] *School of Materials Science and Engineering, Anhui University, Hefei, 230601, China*

† Electronic supplementary information (ESI) available: Synthesis, characterization, ^{1}H NMR, spectroscopic data and other materials. See DOI: https://doi.org/10.1039/d2cc05787e

Scheme 1 Schematic representation for supramolecular chirogenesis on the basis of the optically active Pt(II) metallotweezers **1**. The counteranions are tetrafluoroborate (BF_4^-) in the structure of **1**.

stereogenic center was embedded in the side chains,[11] herein, four (1*R*)-pinene units are fused to the Pt(II) terpyridine pincers in **1** to strengthen the supramolecular chirogenic signals.[12] Interestingly, **1** is prone to associate with other molecules of **1** to form a self-complexed structure (Scheme 1). A stereo-specific twist is generated because of the stacking of Pt(II) terpyridine [Pt(II)(N^N^N)] pincers, giving rise to the emergent chiroptical signals in the MLCT/LLCT absorption region. With the addition of compound **2** (Scheme 1) as the complementary guest, the self-complexation structure of **1** converts to the sandwich complex **1⊃2**. This consequently leads to the chirogenic signal in the MMLCT absorption region, thanks to the participation of Pt(II)–Pt(II) metal–metal interactions for the host–guest entity. Accordingly, dual supramolecular chirogenic signals form in the visible region, by taking advantage of the diverse complexation modes of the Pt(II) metallotweezers.

We first studied self-complexation behavior of the Pt(II) metallotweezers **1**. In chloroform, protons H_2 and H_3 displayed downfield shifts upon varying the concentration from 0.20 mM to 20.0 mM (Fig. S12, ESI†). Concentration-dependent ^{1}H NMR measurements provided the self-association constant of 5.34×10^2 M^{-1} (±34%) for **1** (Fig. S13, ESI†). Generally, two possible self-aggregation modes exist for metallotweezers (Fig. S14, ESI†). One is the mutual stacking of pincer units in a quadruple manner.[8e] The other is sandwiching of the spacer unit into the cavity of the complementary tweezers.[8f] The latter mode is excluded in the case of metallotweezers **1**, since the non-planar diphenylpyridine spacer is unable to be encapsulated into the cavity. The self-complexed structure of **1** was clarified *via* density functional theory (DFT) computations. Two quadruple stacking structures might form for **1**, namely head-to-tail and head-to-head binding modes for the neighbouring Pt(II)(N^N^N) pincers (Fig. S15, ESI†). For the optimized geometries, the head-to-head binding mode (Fig. 1a) featured a lower Gibbs free energy than that of the head-to-tail mode ($\Delta E = 0.974$ kcal mol^{-1}, Fig. S15, ESI†). The π–π distances between the Pt(II)(N^N^N) pincers are 3.29 Å, 3.47 Å, and 3.29 Å, respectively. Apparently, the pre-organization effect of the rigid diphenylpyridine spacer, together with the strong stacking tendency of the Pt(II)(N^N^N) pincers, guarantees formation of the self-complexation structure for **1**. Formation of the head-to-head binding structure was further demonstrated *via* [1]H–[1]H ROESY measurements. In particular, strong correlations exist between protons H_4/H_5 and H_4/H_6 (Fig. S16a, ESI†), which are absent in the ^{1}H–^{1}H COSY spectrum (Fig. S16b, ESI†) under the same conditions.

The spectroscopic properties were further examined for **1**. In dilute chloroform (*c* = 0.10 mM), only 8.9% of **1** existed in the complexed form, denoting the dominance of the monomeric state. The visible light absorbance ranged between 378 and 510 nm ($\varepsilon = 9.07 \times 10^3$ M^{-1} cm^{-1} at 395 nm, Fig. 1b), while the emission signal was centred at 560 nm (Fig. S17, ESI†). With reference to previous reports,[9] these signals were assigned to the admixture of metal-to-ligand and ligand-to-ligand charge-transfer (MLCT/LLCT) transitions of the alkynyl Pt(II)(N^N^N) moiety. Upon switching the solvent from chloroform to

Fig. 1 (a) Optimized structure of the self-complexed dimer **1₂**. (b) Absorption spectra of **1** in acetonitrile (red line) and chloroform (black line) (*c* = 0.10 mM). (c) Degree of α_{agg} for **1** monitored at 500 nm *versus* different temperatures (*c* = 0.10 mM in acetonitrile). Inset: van't Hoff plot fitting for the self-complexation process of **1**. (d) Temperature-dependent CD spectra of **1** (*c* = 0.10 mM in acetonitrile). The arrows indicate the spectral change upon decreasing the temperature.

acetonitrile, the MLCT/LLCT emission signal declined for the intensity (Fig. S17, ESI†). Moreover, a low-energy shoulder band emerged for **1** ($\varepsilon = 1.70 \times 10^3$ M^{-1} cm^{-1} at 510 nm, Fig. 1b). These phenomena suggest a stronger self-complexation capability in acetonitrile. This could be ascribed to the association of the dimer **1₂** into the oligomeric species, considering that π–π stacking interactions are stronger in acetonitrile than those in chloroform.[13] The conclusion is manifested by the broadened ^{1}H NMR peaks (Fig. S18, ESI†), together with the larger hydrodynamic diameter from DLS measurements (Fig. S19, ESI†).

The intensity of the low-energy band between 510 and 600 nm declined upon increasing the temperature to 353 K, with an isosbestic point at 463 nm (Fig. S20, ESI†). The results support the reversible conversion between the monomeric state at high temperature and the complexed state at low temperature. The equal *K* model[14] was employed to fit the melting curves, acquired by plotting the absorption intensity changes at 500 nm *versus* the temperature (Fig. 1c). The T_m values [the temperature at which the degree of aggregation (α_{agg}) is 0.5] increased at higher monomer concentrations (T_m: 288 K at 2.50×10^{-5} M *versus* 306 K at 2.00×10^{-4} M, Fig. S20, ESI†). According to a modified van't Hoff plot (Fig. 1c, inset), the enthalpy (ΔH) and entropy (ΔS) values were determined to be -84.7 kJ mol^{-1}, and -206 J mol^{-1} K^{-1}, respectively. Accordingly, this provided the self-complexed binding constant of 1.29×10^4 M^{-1} at 298 K, which is much higher than that in chloroform [5.34×10^2 M^{-1} (±34%)]. We rationalized that the higher self-complexion affinity in acetonitrile involved not only the dimeric stacking but the hierarchical association into oligomeric species.

Since the self-complexed structure adopts a head-to-head binding mode, it provides asymmetry by transferring chirality from the (1*R*)-pinenes to the Pt(II)(N^N^N) pincers. As can be seen, a weak Cotton effect below 419 nm exists for **1** at 353 K (Fig. 1d), supporting the origin of the molecular chirality from the (1*R*)-pinene units (Fig. S21, ESI†). Upon decreasing the temperature to 298 K, a bisignate CD signal appeared for **1** in the low-energy MLCT/LLCT absorption region (418–550 nm), with the positive maximum at 489 nm ($\Delta\varepsilon = 2.04$ mol^{-1} cm^{-1}) and the negative maximum at 437 nm ($\Delta\varepsilon = -1.89$ mol^{-1} cm^{-1}, Fig. 1d). Accordingly, the self-complexation of **1** prevents carbon–carbon and carbon–platinum bond rotations, exerting a crucial impact on the supramolecular chirogenic behavior. The conclusion is further demonstrated by the weakened Cotton effect in chloroform due to its weakened self-complexation tendency (Fig. S24, ESI†).

After elucidating the self-complexation properties of **1**, we turned to its host–guest complexation behavior. According to electrospray ionization mass spectrometry, an *m/z* value of 2501.85 was observed for **1**⊃**2**, corresponding to $[1 + 2 + H]^+$. The color of **1** in acetonitrile solution changed from yellow to orange upon adding the charge-neutral guest **2** in an equivalent ratio (Fig. S26a, ESI†). A new absorption band emerged in the low energy region, ranging from 500 to 650 nm (Fig. 2a). This is a characteristic of metal–metal-to-ligand charge-transfer (MMLCT) transitions.[10] Simultaneously, the MLCT/LLCT emission at 578 nm declined in its intensity, with a concomitant increase in the MMLCT emission band at 786 nm (Fig. S26b, ESI†). Depending on the molar ratio plot (Fig. S27, ESI†), the binding stoichiometry between the metallotweezer receptors **1** and guest **2** was 1 : 1. By fitting the collected UV/Vis absorbances at 510 nm, 525 nm and 540 nm, the "apparent" constant (K_d) value was determined to be 3.75×10^5 M^{-1} ($\pm27\%$) in acetonitrile at 298 K (Fig. 2a, inset). Since the self-complexation of **1** was involved in the titration process, the "real" binding constant (K_a) value for **1**⊃**2** was 6.96×10^4 M^{-1} ($\pm13\%$) (eqn (S11), ESI†).[15] This value was higher than that in chloroform [K_a: 1.85×10^3 M^{-1} ($\pm3.2\%$), Fig. S29, ESI†]. Although the K_a value of **1**⊃**2** was smaller when observed *via* ^{1}H NMR titration experiments [9.32×10^3 M^{-1} ($\pm28\%$),

Fig. S30 and S31, ESI†], the value was also higher than that in chloroform [K_a: 2.54×10^3 M^{-1} ($\pm24\%$), Fig. S32 and S33, ESI†].

The energy-minimized structure of complex **1**⊃**2** was elucidated *via* DFT calculations. As expected, **2** is encapsulated into the cavity of the metallotweezers **1** to form a sandwiched complex (Fig. 2b). The inter-planar π-distances between **2** and the two Pt(II)(N^N^N) pincers on **1** are determined to be 3.30 Å and 3.21 Å, validating the presence of two-fold π–π stacking interactions. This conclusion was further validated *via* ^{1}H NMR experiments. Upon addition of one equivalent of **2** to **1**, the ^{1}H NMR resonances of protons H_1 and H_2 shifted upfield ($\Delta\delta = -0.36$ and -0.58 ppm, respectively), while protons H_4 varied from 8.43 ppm to 8.71 ppm because of the deshielding effect (Fig. S32, ESI†). Meanwhile, the Pt–Pt distances between **1** and **2** are 3.51 and 3.22 Å, respectively. This supports the existence of Pt(II)–Pt(II) interactions in complex **1**⊃**2**, and is highly consistent with the emergence of the MMLCT absorption and emission signals (Fig. S26a and S26b, ESI†).

The participation of two-fold Pt(II)–Pt(II) and π–π stacking interactions contributes to the high binding affinity for complex **1**⊃**2**. When the control compound **3** (Fig. S21, ESI,† inset) with the mono-nuclear Pt(II)(N^N^N) unit was employed as the host instead of **1**, the K_a value for the resulting complex **3**⊃**2** decreased to be 15.9 M^{-1} M^{-1} (Fig. S34 and S35, ESI†), two orders of magnitude lower than that of complex **1**⊃**2**. When the temperature was elevated to 353 K, the K_a value of complex **1**⊃**2** in acetonitrile was determined to be 3.21×10^4 M^{-1} ($\pm5.9\%$) (Fig. S38, ESI†), reaching one half of the value at 298 K. The high binding affinity of **1**⊃**2** at elevated temperature is ascribed to the weakening of the **1** self-complexation strength upon heating. This buffers the decreased host–guest complexation, and thereby the strong complexation between **1** and **2** persists.

We further investigated the supramolecular chirogenic signal for the resulting host–guest complex. Upon the gradual addition of **2** into an acetonitrile solution of **1**, the positive CD signal located at 497 nm became negative ($\Delta\varepsilon$: from 1.79 mol^{-1} cm^{-1} to -3.18 mol^{-1} cm^{-1}, Fig. 3a and Fig. S39, ESI†). Meanwhile, the Cotton effect appeared in the MMLCT absorption region ($\Delta\varepsilon = +1.18$ mol^{-1} cm^{-1} at 570 nm). In stark contrast, a negligible Cotton effect was observed when employing **3** instead of **1** (Fig. S40a, ESI†), because of the weak complexation strength of complex **3**⊃**2**. Accordingly, metallotweezers/guest complexation
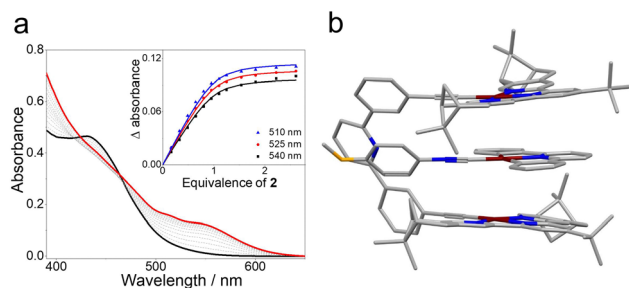
Fig. 2 (a) UV/Vis absorbance changes of **1** at 298 K ($c = 0.05$ mM in CH$_3$CN) upon the progressive addition of **2**. Inset: intensity changes in UV/Vis absorbance at 510 nm, 525 nm, and 540 nm. The solid lines were obtained *via* a Matlab-based global analysis program. (b) Optimized structure of the host–guest complex **1**⊃**2** on the basis of DFT calculations.
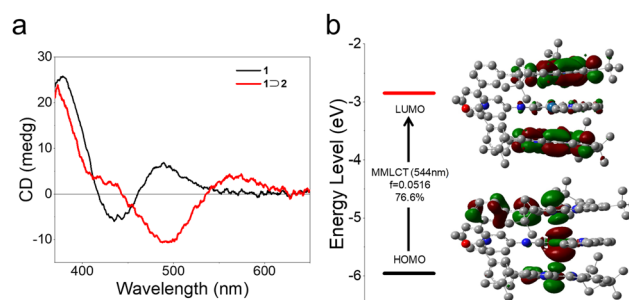
Fig. 3 (a) CD spectra of **1** and **1**⊃**2** at 298 K ($c = 0.10$ mM for each compound in CH$_3$CN). (b) Energy-level diagram of **1**⊃**2** *via* TD-DFT computations.

with sufficient binding affinity is a prerequisite for supramolecular chirogenesis. The Cotton shape of $1 \supset 2$ was maintained at elevated temperatures because of the robust host–guest complexation, despite the decreased CD intensities (at 497 nm: $\Delta \varepsilon = |1.26|$ cm^{-1} M^{-1} at 353 K versus $|3.18|$ cm^{-1} M^{-1} at 298 K, Fig. S41, ESI†).

The origin of the low-energy supramolecular chiroptical signals (ranging from 444 nm to 624 nm) was clarified using time-dependent density functional theory (TD-DFT) calculations. As shown in Fig. 3b, the electron density of the LUMO is distributed over the Pt(II)(N^N^N) pincers of 1. Meanwhile, the electron density of the HOMO is mainly distributed on the 5d$_{z^2}$ orbitals of the Pt(II) atoms in both 1 and 2. Accordingly, the theoretical Cotton effect in the low-energy absorption region is composed of HOMO → LUMO transitions (composition: 76.6% at 544 nm), belonging to metal–metal-to-ligand charge transfer (MMLCT) transitions. For most of previous host–guest systems, supramolecular chirogenic signals arose from the individual or conjoint non-covalent forces of metal–ligand coordination, hydrogen bonding, π–π stacking, and hydrophobic interactions. Complex $1 \supset 2$ represents a rare type of supramolecular chirogenic system with the involvement of Pt(II)–Pt(II) metal–metal interactions.[16]

In summary, metallotweezer 1 with optically active Pt(II)(N^N^N) pincers prefers to form a self-complexed structure via a head-to-head binding mode, leading to supramolecular chirogenic signals in the MLCT/LLCT absorption region. Furthermore, a metallotweezers/guest complex forms upon adding the complementary guest 2 into 1. This is accompanied by the formation of Pt(II)–Pt(II) metal–metal interactions, and thereby induces supramolecular chirogenesis in the MMLCT transition region. Therefore, a dual supramolecular chirogenic system in the visible region has been successfully constructed by taking advantage of the diverse complexation modes of Pt(II) metallotweezers.

Conflicts of interest

There are no conflicts to declare.

Notes and references

1 H.-E. Lee, H.-Y. Ahn, J. Mun, Y. Y. Lee, M. Kim, N. H. Cho, K. Chang, W. S. Kim, J. Rho and K. T. Nam, *Nature*, 2018, **556**, 360.
2 (a) E. Yashima, N. Ousaka, D. Taura, K. Shimomura, T. Ikai and K. Maeda, *Chem. Rev.*, 2016, **116**, 13752; (b) L. Zhang, H. Wang, S. Li and M. Liu, *Chem. Soc. Rev.*, 2020, **49**, 9095; (c) D.-W. Zhang, M. Li and C.-F. Chen, *Angew. Chem., Int. Ed.*, 2022, **61**, e202213130.
3 (a) V. V. Borovkov, J. M. Lintuluoto and Y. Inoue, *J. Am. Chem. Soc.*, 2001, **123**, 2979; (b) G. Proni, G. Pescitelli, X. Huang, K. Nakanishi and N. Berova, *J. Am. Chem. Soc.*, 2003, **125**, 12914; (c) V. V. Borovkov, G. A. Hembury and Y. Inoue, *Acc. Chem. Res.*, 2004, **37**, 449; (d) S. J. Wezenberg, G. Salassa, E. C. Escudero-Adan, J. Benet-Buchholz and A. W. Kleij, *Angew. Chem., Int. Ed.*, 2011, **50**, 713;
(e) I. C. Pintre, S. Pierrefixe, A. Hamilton, V. Valderrey, C. Bo and P. Ballester, *Inorg. Chem.*, 2012, **51**, 4620; (f) S. A. Ikbal, S. Brahma and S. P. Rath, *Chem. Commun.*, 2015, **51**, 895; (g) M. Liu, Y. Han, H. Zhong, X. Zhang and F. Wang, *Angew. Chem., Int. Ed.*, 2021, **60**, 3498.
4 (a) L. Wang, Z. Chen, W. Liu, H. Ke, S. Wang and W. Jiang, *J. Am. Chem. Soc.*, 2017, **139**, 8436; (b) H. Zhu, Q. Li, Z. Gao, H. Wang, B. Shi, Y. Wu, L. Shangguan, X. Hong, F. Wang and F. Huang, *Angew. Chem., Int. Ed.*, 2020, **59**, 10868; (c) H. Liang, B. Hua, F. Xu, L.-S. Gan, L. Shao and F. Huang, *J. Am. Chem. Soc.*, 2020, **142**, 19772; (d) S. Yu, Y. Wang, S. Chatterjee, F. Liang, F. Zhu and H. Li, *Chin. Chem. Lett.*, 2021, **32**, 179; (e) H. Nian, L. Cheng, L. Wang, H. Zhang, P. Wang, Y. Li and L. Cao, *Angew. Chem., Int. Ed.*, 2021, **60**, 15354; (f) H. Zhang, L. Cheng, H. Nian, J. Du, T. Chen and L. Cao, *Chem. Commun.*, 2021, **57**, 3135; (g) C. Tu, W. Wu, W. Liang, D. Zhang, W. Xu, S. Wan, W. Lu and C. Yang, *Angew. Chem., Int. Ed.*, 2022, **61**, e202203541; (h) W.-L. Zhao, Y.-F. Wang, S.-P. Wan, H.-Y. Lu, M. Li and C.-F. Chen, *CCS Chem.*, 2022, **4**, 3540.
5 (a) F. J. Rizzuto, P. Prohm, A. J. Plajer, J. L. Greenfield and J. R. Nitschke, *J. Am. Chem. Soc.*, 2019, **141**, 1707; (b) B. Li, B. Zheng, W. Zhang, D. Zhang, X. Yang and B. Wu, *J. Am. Chem. Soc.*, 2020, **142**, 6304; (c) L. Cheng, K. Liu, Y. Duan, H. Duan, Y. Li, M. Gao and L. Cao, *CCS Chem.*, 2020, **2**, 2749; (d) Y. Ding, C. Shen, F. Gana, J. Wang, G. Zhang, L. Li, M. Shu, B. Zhu, J. Crassous and H. Qiu, *Chin. Chem. Lett.*, 2021, **32**, 3988; (e) D. Chu, W. Gong, H. Jiang, X. Tang, Y. Cui and Y. Liu, *CCS Chem.*, 2022, **4**, 1180.
6 (a) G. Zhang, P. Li, Z. Meng, H. Wang, Y. Han and C. Chen, *Angew. Chem., Int. Ed.*, 2016, **55**, 5304; (b) D. Zheng, C. Yu, L. Zheng, Y. Zhan and H. Jiang, *Chin. Chem. Lett.*, 2020, **31**, 673.
7 J. L. Greenfield, J. Wade, J. R. Brandt, X. Shi, T. J. Penfold and M. J. Fuchter, *Chem. Sci.*, 2021, **12**, 8589.
8 (a) Y. Tanaka, K. M.-C. Wong and V. W.-W. Yam, *Chem. Sci.*, 2012, **3**, 1185; (b) Y. Tian, Y. Shi, Z. Yang and F. Wang, *Angew. Chem., Int. Ed.*, 2014, **53**, 6090; (c) Z. Gao, Y. Han, Z. Gao and F. Wang, *Acc. Chem. Res.*, 2018, **51**, 2719; (d) Y. Tian, B. Chen, S. Jang, M. Yuan, J. Ren and F. Wang, *Chem. Commun.*, 2021, **57**, 11996; (e) Z. Li, Y. Han, Z. Gao and F. Wang, *ACS Catal.*, 2017, **7**, 4676; (f) M. Yuan, X. Zhang, Y. Han, F. Wang and F. Wang, *Inorg. Chem.*, 2020, **59**, 14134.
9 (a) S. Ibanez, M. Poyatos and E. Peris, *Angew. Chem., Int. Ed.*, 2017, **56**, 9786; (b) S. Ibanez, M. Poyatos and E. Peris, *Angew. Chem., Int. Ed.*, 2018, **57**, 16816; (c) N. Hisano, S. Akine, S. Kihara and T. Haino, *Macromolecules*, 2019, **52**, 6160; (d) S. Ibanez, M. Poyatos and E. Peris, *Acc. Chem. Res.*, 2020, **53**, 1401; (e) J. Y.-W. Yeung, F. K.-W. Kong, F. K.-W. Hau, M. H.-Y. Chan, M. Ng, M.-Y. Leung and V. W.-W. Yam, *Angew. Chem., Int. Ed.*, 2022, **61**, e202207313; (f) D. Jia, H. Zhong, S. Jiang, R. Yao and F. Wang, *Chin. Chem. Lett.*, 2022, **33**, 4900; (g) H. Zhong, S. Jiang, L. Ao, F. Wang and F. Wang, *Inorg. Chem.*, 2022, **61**, 7111.
10 (a) V. W.-W. Yam, V. K.-M. Au and S. Y.-L. Leung, *Chem. Rev.*, 2015, **115**, 7589; (b) X. Zhang, Y. Han, G. Liu and F. Wang, *Chin. Chem. Lett.*, 2019, **30**, 1927; (c) Z. Wei, Z. Kang, C. K. Kim, S. Tan, S. Wang, L. Wang, J. Lie and Y. Wang, *Chin. Chem. Lett.*, 2021, **32**, 493.
11 (a) T. Ikeda, M. Takayama, J. Kumar, T. Kawai and T. Haino, *Dalton Trans.*, 2015, **44**, 13156; (b) A. Aliprandi, C. M. Croisetu, M. Mauro and L. D. Cola, *Chem. – Eur. J.*, 2017, **23**, 5957; (c) Z.-L. Gong and Y.-W. Zhong, *Sci. China: Chem.*, 2021, **64**, 788.
12 X.-P. Zhang, V. Y. Chang, J. Liu, X.-L. Yang, W. Huang, Y. Li, C.-H. Li, G. Muller and X.-Z. You, *Inorg. Chem.*, 2015, **54**, 143.
13 Z. Chen, A. Lohr, C. R. Saha-Moller and F. Wurthner, *Chem. Soc. Rev.*, 2009, **38**, 564.
14 R. B. Martin, *Chem. Rev.*, 1996, **96**, 3043.
15 G. B. W. L. Ligthart, H. Ohkawa, R. P. Sijbesma and E. W. Meijer, *J. Am. Chem. Soc.*, 2005, **127**, 810.
16 (a) S. Y.-L. Leung, W. H. Lam and V. W.-W. Yam, *Proc. Natl. Acad. Sci. U. S. A.*, 2013, **110**, 7986; (b) C. Lochenie, A. Insuasty, T. Battisti, L. Pesce, A. Gardin, C. Perego, M. Dentinger, D. Wang, G. M. Pavan, A. Aliprandi and L. D. Cola, *Nanoscale*, 2020, **12**, 21359; (c) Z. Gao, Y. Tian, H.-K. Hsu, Y. Han, Y.-T. Chan and F. Wang, *CCS Chem.*, 2021, **3**, 105.